FULL RESEARCH ARTICLE

Effects of post-printing heat treatment on microstructure, corrosion and wet wear behavior of CoCrW alloy produced by L-PBF process

A. Lanzutti[1] · F. Andreatta[1] · E. Vaglio[1] · M. Sortino[1] · G. Totis[1] · L. Fedrizzi[1]

Abstract

CoCr alloys are widely used as human implants because of both their superior corrosion resistance and superior mechanical properties (fatigue, wear resistance, etc.) respect to other metal alloys used in biomedical field. In particular, CoCrW alloys are used mainly to produce dental implants. In this study, the effects of thermal treatment on the corrosion resistance and wet wear resistance of CoCrW alloys produced via Laser-Powder Bed Fusion (L-PBF) were investigated, and the corrosion resistance and wet wear resistance of the L-PBF specimens were compared with those of the specimens obtained after forging. The heat treatment involved the solubilization of the alloy at 1150 °C in an Ar-saturated atmosphere, followed by furnace cooling. A detailed microstructural characterization of the L-PBF specimens was carried out using a light microscope and a scanning electron microscope in both the horizontal and vertical growth directions. Scanning Kelvin probe measurements were performed on the heat-treated specimens obtained by three-dimensional printing and forging. The void contents of the specimens were evaluated using the Archimedes' method and image analysis. Vickers (HV2) hardness measurements were performed to evaluate the mechanical properties of the specimens. The corrosion properties of the specimens were evaluated by carrying out potentiodynamic tests in two different corrosive media (aqueous solution (9 g/L NaCl) at pH=2 and 7). The corroded areas of the specimens were then examined using scanning electron microscopy (SEM). Finally, tribological tests were performed using the pin (Ti counter material)-on-flat configuration under dry and wet conditions, using the same corrosive environments as those used in the potentiodynamic tests and two different stroke lengths. The worn samples were characterized using SEM to investigate their wear mechanisms, and a stylus profilometer was used to determine the wear rates of the materials. The experimental results showed that the additively manufactured CoCrW L-PBF alloy had higher corrosion resistance than the wrought material. In addition, the additively manufactured material showed better dry and wet wear performances than the wrought material. Nevertheless, the heat treatment did not affect the properties evaluated in this study.

Keywords L-PBF · CoCrW alloy · Corrosion · Wet-wear · Post-printing heat treatment

1 Introduction

CoCr alloys are widely used as biomaterials for several prostheses that require good mechanical properties (such as fatigue and wear) and good corrosion resistance [1–5], such as dental prostheses, hip prostheses, and knee implants.

The main CoCr families used in these applications are CoCrMo alloys, which are widely used for several types of prostheses [2, 4], and CoCrW alloys are mainly used in dental prostheses because of their good bonding with porcelains [6, 7]. Both the alloys can be produced via conventional technological processes, such as forging [2, 4], or by means of additive manufacturing techniques, in particular, powder bed fusion techniques such as electron beam melting [8] and LASER-Powder Bed Fusion (L-PBF) [6, 7, 9–15]. Usually, implants produced with these alloys suffer from degradation related to corrosion fatigue [4], wear [2], or only corrosion [1, 2] aggravated by the local acidification of physiological media due to inflammation or the presence of crevices [4].

The microstructure of CoCrW alloys produced by L-PBF is usually composed of a γ matrix with a small fraction of the epsilon phase. The amount of the epsilon phase in such alloys is generally restrained owing to the brittleness that this phase can induce in the material [7, 12, 13]. On the

✉ A. Lanzutti
alex.lanzutti@uniud.it

1   Polytechnic Department of Engineering and Architecture (DPIA), University of Udine, via Delle Scienze 208, 33100 Udine, Italy

contrary, Hitzler et al. did not find the epsilon phase in as-built materials produced using the L-PBF process; however, they found this phase in heat-treated samples [16]. On the other hand, it has been reported that the presence of small amounts of fine-grained epsilon phase, as found in L-PBF alloys, can increase the mechanical response of the material in terms of tensile properties, although certain anisotropy is observed [12]. Some deleterious effects of the epsilon phase on the mechanical properties of samples produced by the L-PBF technique were observed by Wang et al. [17]. They noticed that the properties of the material deteriorated with an increase in the powder recycling time. This decrease in the mechanical properties is related to the production of spatter particles that affected the quality of the material, mainly in terms of porosity.

In terms of corrosion properties, the CoCrW alloys produced by L-PBF exhibited good corrosion resistance, which slightly depended on the laser scanning path geometry.

Many works were published to determine the effect of heat treatment on CoCrMo alloys [18, 19] on microstructure and mechanical properties, although both microstructure and mechanical properties are pretty different from the CoCrW alloys. On the other hand, these effects were not intensively studied in other works on CoCrW alloys. A study was conducted to investigate the effect of a post-printing heat treatment on the corrosion properties of these alloys [10, 12]. The reference treatment for these alloys involved annealing at 1150 °C, followed by cooling in a furnace. When the tests were performed in artificial saliva containing F ions, the corrosion resistance decreased owing to the production of coarse Si-W precipitates. The heat treatment also had a negative effect on the tensile and yield strengths of these alloys.

In short, the tribological properties of the alloys produced by additive manufacturing have not been adequately investigated. Some studies have been carried out for investigating the tribological properties of Co alloys containing W produced by conventional methods by performing tests at high temperatures [20] or in wet conditions [21, 22]. In particular, Guadalupe et al. [21] investigated the tribocorrosion properties of many CoCr alloys produced by the forging process in acidic environments. The materials showed good tribocorrosion behavior, although they also underwent a mechanical chemical attack. Luo et al. [22] performed dry sliding tests on CoCr alloys produced by L-PBF and showed that CoCrW exhibited the worst wear behavior. The tribological properties of this material improved with the addition of Cu as an alloying element. This element increased the epsilon phase content of the material, thus improving its hardness and tribological properties. In the biomedical field, the addition of Cu also enhances the antibacterial properties of biomaterials [13, 14, 22].

The aim of this study is to investigate the corrosion and wet-wear properties of additively manufactured CoCrW alloy and comparing them with the properties of the wrought material, with the same chemical composition, used as a reference, by considering the effects of heat treatment and growth direction. The corrosion and wear performances of the CoCrW alloy were investigated in neutral and acidic physiological media to evaluate their potential for application in dental or biomedical implants. In particular, this work aims to determine the possible differences between additively manufactured materials and conventionally produced materials.

2 Experimental procedures

2.1 Sample preparation

A commercial CoCrW powder (Remanium Star CL) was used for producing the additively manufactured samples. The chemical compositions of the CoCrW samples, as determined using optical spectroscopy (Rf-GDOES, Horiba Jobin Yvon, sensibility of 50 ppm, performed on as machined samples) and gas-in-metal analysis (Leco CS844 and Leco ON 836, performed on 10 g specimens extracted from machined samples) are listed in Table 1.

The CoCoW powder consisted of spherical particles (Fig. 1) with a granulometric distribution ranging from 11.13 (10th %ile) to 32.89 μm (90th %ile) and a median diameter of 19.48 μm (Fig. 1 a). No defects such as voids or blows were detected in the metal powders.

A total of 120 parallelepiped specimens (dimensions: 30.5 mm × 20.5 mm × 7 mm) were prepared, half of which were oriented horizontally, while the others were oriented vertically (Fig. 2). For each orientation, 30 samples. The specimens were randomly distributed on the building platform. To achieve uniform layer deposition, the 3D printed specimens were positioned at 45° with respect to the recoating direction.

The samples were produced using a Concept Laser M2 Cushing machine (single-mode CW ytterbium-doped fiber

Table 1 Chemical compositions (wt%) of the CoCrW samples

	Cr	W	Si	C (ppm)	O (ppm)	S (ppm)	N (ppm)	Co
Additively manufactured	27.6	9.1	1.43	0.005	61	15	148	Bal
Wrought material	28.1	8.8	1.45	0.005	20	16	40	Bal
Chemical composition range	28	9	1.5	–	–	–	–	Bal
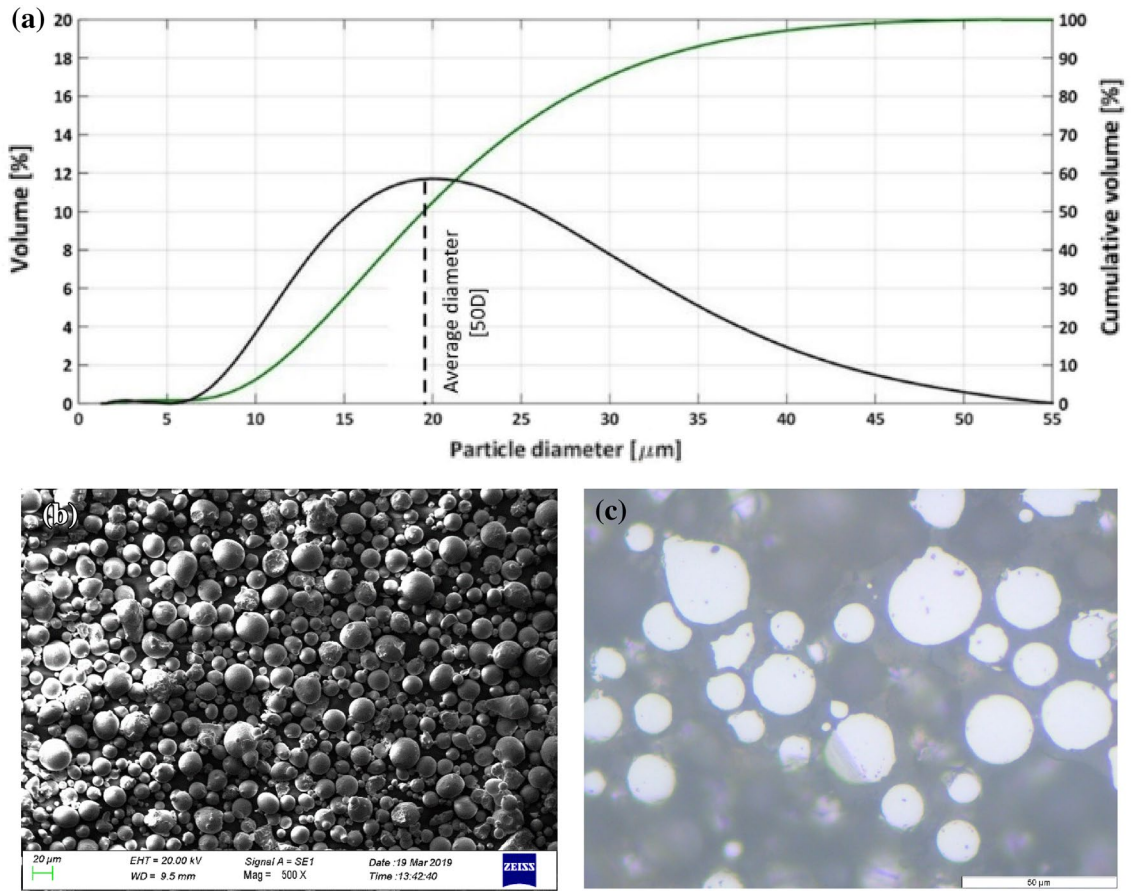
Fig. 1 **a** Granulometric distribution of the CoCrW alloy powder (Horiba LA950 laser scattering PSD analyzer) **b** SEM micrograph of the powders used in this study. **c** Light microscopy analysis of the powders
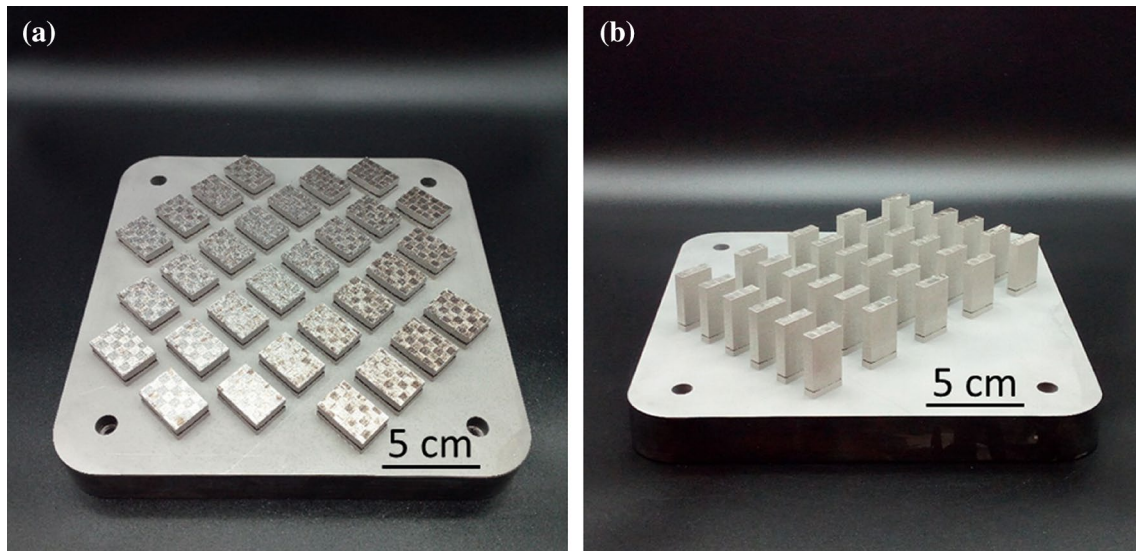
Fig. 2 **a** Horizontal and **b** vertical samples produced for experimental investigation

Table 2 Technological parameters used to print the samples

	Specimens	Support structures
Power	160 W	60 W
Scanning speed	800 mm/s	400 mm/s
Spot diameter	125 μm	125 μm
Hatch distance	70 μm	–
Layer thickness	30 μm	30 μm

laser with a wavelength of 1070 nm) under an inert argon atmosphere with less than 0.2% residual oxygen. Table 2 lists the main technological parameters used to print the specimens investigated in this study, using optimized printing conditions suggested by Concept Laser.

The laser scan path consisted of a chessboard pattern with 5 mm × 5 mm squares scanned along two mutually perpendicular directions. The adjacent islands were spaced 70 μm apart, and each of them underwent an angular rotation of 90° and an XY plane drift of 1 mm at each layer to promote structural evenness within the processed material. No contour was scanned to avoid the modification of the surface properties of the tested material.

After the production, half of the samples were heat-treated. In the heat treatment, the samples were heated at 1100 °C for 1 h in an Ar-saturated atmosphere, followed by cooling to 300 °C in a furnace. The heat treatment procedure was recommended by the powder producer for specific applications in the field of dentistry (simulating the ceramic firing process for the dental implants) [23, 24].

After the heat treatment, the additively manufactured samples were machined through conventional milling (CNC HAAS VF2-TR, by using a machining optimized procedure for CoCr alloys) to obtain flat specimens (20 mm × 30 mm × 5 mm) for tribological measurements. The sample surface roughness was 0.2 μm (Ra) (Stylus profilometer Dektak 150, 3 measurements each sample (scan length of 4 mm sampling length of 0.1 mm, cut off 0.1 mm)).

A CoCrW wrought material (Dentarum Remanium star MD II) with a chemical composition same as that of the powders used in this study (Table 1) was considered as the main reference for the final comparison. The material was machined to achieve dimensions and surface roughness same as those of the additively manufactured specimens. The wrought samples were analyzed under the as-delivered conditions without thermal treatment.

2.2 Microstructural characterization

All the L-PBF and wrought samples were subjected to metallographic preparation. For all the samples, the analyzed area was the largest side of the parallelepiped for both the horizontal and vertical build directions. Subsequently, the additively manufactured samples were characterized prior to the acid etching process in order to estimate their void contents by means of both image analysis (before etching) and the Archimedes' method on three samples for each tested condition. The %defect distribution was evaluated analyzing the ratio between the total defects for one dimensional class on total defects on three surfaces for each experimental condition (20 × 5 mm). The samples were electrolytically etched in a solution of water and HCl with water:HCl ratio = 1:9. The etching was performed under a potential control at 3 V for 60 s using a graphite bar as the cathode. The as-printed, heat-treated, and wrought samples were subsequently analyzed by light microscopy (Olympus GX 71) to observe their microstructural evolution. The samples were then subjected to field emission electron microscopy energy-dispersive X-ray spectroscopy (FE-SEM-EDXS) (JSM 7200F + INCA Ultimax) analysis to examine the shape and distribution of precipitates and to further investigate the microstructure of the additively manufactured materials before and after the heat treatment. Scanning Kelvin probe force microscopy (SKPFM) was employed to evaluate the Volta potential distribution on the surface of the L-PBF samples. This method is very useful for correlating the microstructure of a material with its corrosion properties [4, 25, 26]. The Volta potential maps of the samples were acquired using atomic force microscopy (AFM) (Nanoscope III multimode + Extender TM electronic module). The maps were recorded at room temperature with a relative humidity of 45–70%. The tips used were n + Si coated with PtIr5. The samples were scanned at a frequency of 0.1 Hz, and for the Volta potential maps, the tip was lifted up to 100 nm.

After the microstructural characterization, hardness tests (Vickers hardness with an applied load of 2 kg for 15 s, 3 measurements each sample, Struers Duramin 2) were carried out on the L-PBF samples. Thus, the effects of the heat treatment processes on the samples could be investigated, and the tribological properties of the CoCrW samples could be correlated to their microstructure.
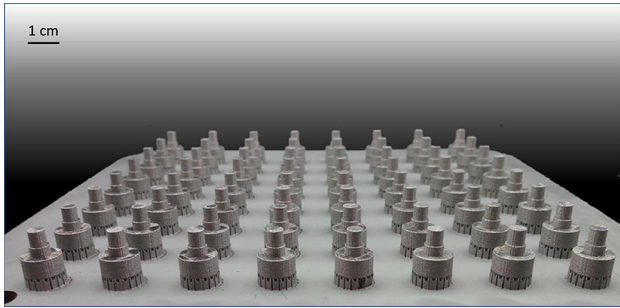
2.3 Corrosion testing

The electrochemical tests of all the L-PBF samples and wrought material were carried out in two distinct electrolytes: an aqueous solution containing 9 g/L of NaCl (pH 7) with pH = 7 and 2. The corrosive medium with neutral pH was a typical physiological solution used to evaluate the corrosion properties of metallic biomaterials, while the medium with pH = 2 was used to simulate the electrochemical behavior in geometrical crevices that can be formed in human implants [1, 3, 4].

A three-electrode electrochemical cell was used to perform the potentiodynamic tests (Metrohm Autolab PGSTAT30 Potentiostat) of the samples. The three

Table 3 Chemical composition of the Ti pins used as counter materials for the wet wear tests

	C	V	N	Ti	Al	Fe	O	H
Pin	0.03	4.11	0.03	Bal	5.88	0.10	0.11	0.006

Fig. 3 Counter materials prepared for tribological tests

Table 4 Process parameters used for the preparation of the titanium counter materials

	Bulk area	Supports
Laser power	225 W	180 W
Scanning speed	1300 mm/s	1300 mm/s
Spot diameter	155 µm	100 µm
Hatch distance	90 µm	–
Layer thickness	25 µm	50 µm

electrodes were: the sample (working electrode), a Pt wire (counter electrode), and an Ag/AgCl electrode (reference electrode). The electrochemical tests of all the samples were carried out after the stabilization of the OCP (Open Circuit Potential) (10 min), starting at -100 mV vs. OCP with a scan rate of 0.2 mV/sec and were stopped at 1 V vs. the reference electrode. The electrochemical tests were carried out in an Avesta cell to avoid possible crevice corrosion. The morphology of the corroded areas, which were obtained after the potentiodynamic tests, was analyzed using a scanning electron microscope equipped with an EDXS probe (Zeiss Evo 40 + INCA X Sight).

2.4 Wet-wear tests

The tribological properties of the additively manufactured samples (under both the as-printed and heat-treated conditions for each printing direction) and wrought material were evaluated. The tests were performed in a pin-on-flat configuration using a CETR UMT 3 tribometer. The instrument was equipped with a 2-axes load cell (capacity: 1 kN). The counter material used in this study was a Ti gr.5alloy (composition is listed in Table 3) produced via L-PBF, which is usually used as a coupling material with CoCr alloys in human modular prostheses [4]. The counter material pins used for the tests (Fig. 3) were additively manufactured using Concept Laser M2 C on the machine used to prepare the CoCrW samples. The Ti powders consisted of spherical particles with diameters ranging from 20.58 (10th %ile) to 47.24 µm (90th %ile), with a median value of 31.43 µm. These powders were processed under an inert argon atmosphere ($O_2 < 0.2\%$) using the process parameters listed in Table 4. The samples were prepared using the island strategy used for preparing the CoCrW samples, and in this case, no contour was scanned. Finally, the titanium pins

were machined using a CNC milling machine to obtain a very smooth contact surface. The hardness of the produced counter materials was 350–400 HV.

For the wear tests, two stroke lengths of 10 and 0.2 mm were used. The applied load was 225 N, and the test frequency was 1 Hz (Hertzian pressure of 11.5 MPa). The tests were performed on three different samples for each tested condition. The load used for the wear tests, and subsequently the relative Hertzian pressure, is in the range of the loads used for the dental applications [27]. The wear tests were performed under dry and wet conditions. In the wet condition, the samples were immersed (15 min before the tests started in the tribometer cell) in the electrolytes used for the corrosion tests at room temperature. During relative sliding, COF (Coefficient Of Friction) was continuously acquired. After the tests, the wet specimens were immersed in ethanol and then dried to avoid further corrosion of the worn area. The worn samples were then analyzed using SEM and EDXS in the proximity of the worn area (top view) to investigate their wear mechanisms. Subsequently, the samples tested at a stroke length of 10 mm were examined using a stylus profilometer (Veeco Dektak 150) to determine their wear rates [28–30] according to Eq. 1:

$$K = \frac{V}{S \cdot F_z},\qquad(1)$$

where V (mm^3) is the volume of the material removed from the sample surface, as calculated using the profilometer, S (m) is the sliding distance, and F_z (N) is the vertical load (applied). The worn area of the specimens tested at the stroke length of 0.2 mm was analyzed using a light stereomicroscope. This procedure has also been used previously

to evaluate the fretting degradation of materials. The experimental conditions used in this study were very close to the fretting wear condition [31, 32].

3 Results and discussion

## 3.1 Preliminary microstructural characterization

As the first step of the microstructural characterization of the samples, their void contents and distributions were analyzed to investigate the relationship between their electrochemical properties and densities. The discontinuities in the additively manufactured CoCrW were mainly small pores and voids with a size of < 20 µm that can be linked to gas evolution during the melting [19, 33]. Only a few discontinuities with larger dimensions could be detected in the analyzed material (Fig. 4), typically associated to small hot tears. The heat treatment did not affect the pore contents and pore size distributions of the samples. The void content of the L-PBF samples was less than 0.2 vol%, as measured using the both the Archimedes' principle and image analysis [13].

The optical micrographs of the L-PBF CoCrW alloy (in the horizontal/vertical directions and for the printed and heat-treated samples) and reference wrought alloy are shown in Fig. 5.

In the as-printed condition, the laser scan paths could be clearly observed in the L-PBF material. The samples built horizontally exhibited a chessboard laser pattern, while the vertical samples showed overlapping melting pools. The thermal treatment significantly affected the microstructure of the as-printed samples. The heat-treated samples showed a rearrangement of the microstructure to

form quasi-equiaxial grains with an irregular boundary, which was the same for the horizontal and vertical build directions. Inside the grains, some small precipitates (dark granules) were observed, which were further investigated using FE-SEM. The grains visible in the additively manufactured specimens were present in the γ phase [16]. On the other hand, the wrought material showed a γ phase coarser than that detected in the additively manufactured material. In addition, the epsilon phase and small randomly dispersed inclusions were present [34]. No precipitates were detected in the wrought material. A detailed characterization of the microstructure of the additively manufactured samples in both the as-printed and heat-treated conditions was carried out using FE-SEM (Fig. 6).

At higher magnifications, the melting pools of the as-printed materials exhibited a mixed cellular/columnar grain microstructure in both the horizontal and vertical directions, with a submicrometric cell size [13]. This cellular structure was a section of a fine columnar structure. Large amounts of small precipitates, with a size of tens of nanometers were observed near the cell boundaries of the as-printed samples. These precipitates, observed mainly in proximity of cell/column boundaries, are mainly small clusters rich in Si and W and were probably the intermetallic phases found also by other authors [10, 13]. It is likely that these particles are produced by local segregation of W and Si at cell/columns boundaries. In contrast, the heat-treated samples showed coarser microstructure with irregular grain boundaries. The precipitates were coarser than those observed in the as-printed condition. Moreover, these precipitates had different shapes and sizes depending on the precipitation site. At the cell boundaries, the precipitates showed a globular shape and had a micrometric size, while they showed a more elongated shape with a submicrometric size in the inner part
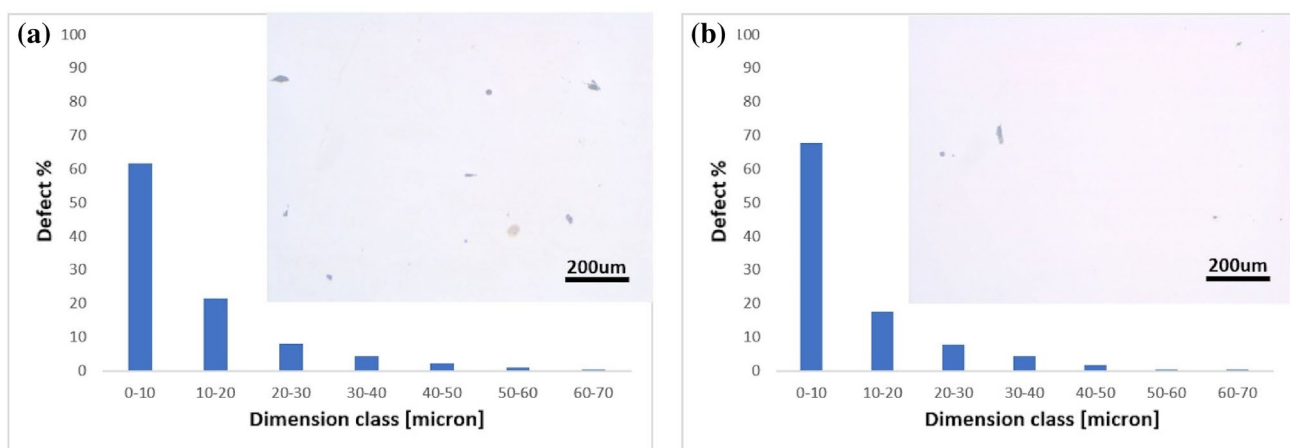
Fig. 4 Void and pore size distributions of the as-printed **a** and heat-treated **b** additively manufactured CoCrW alloys. The pores are indicated by arrows
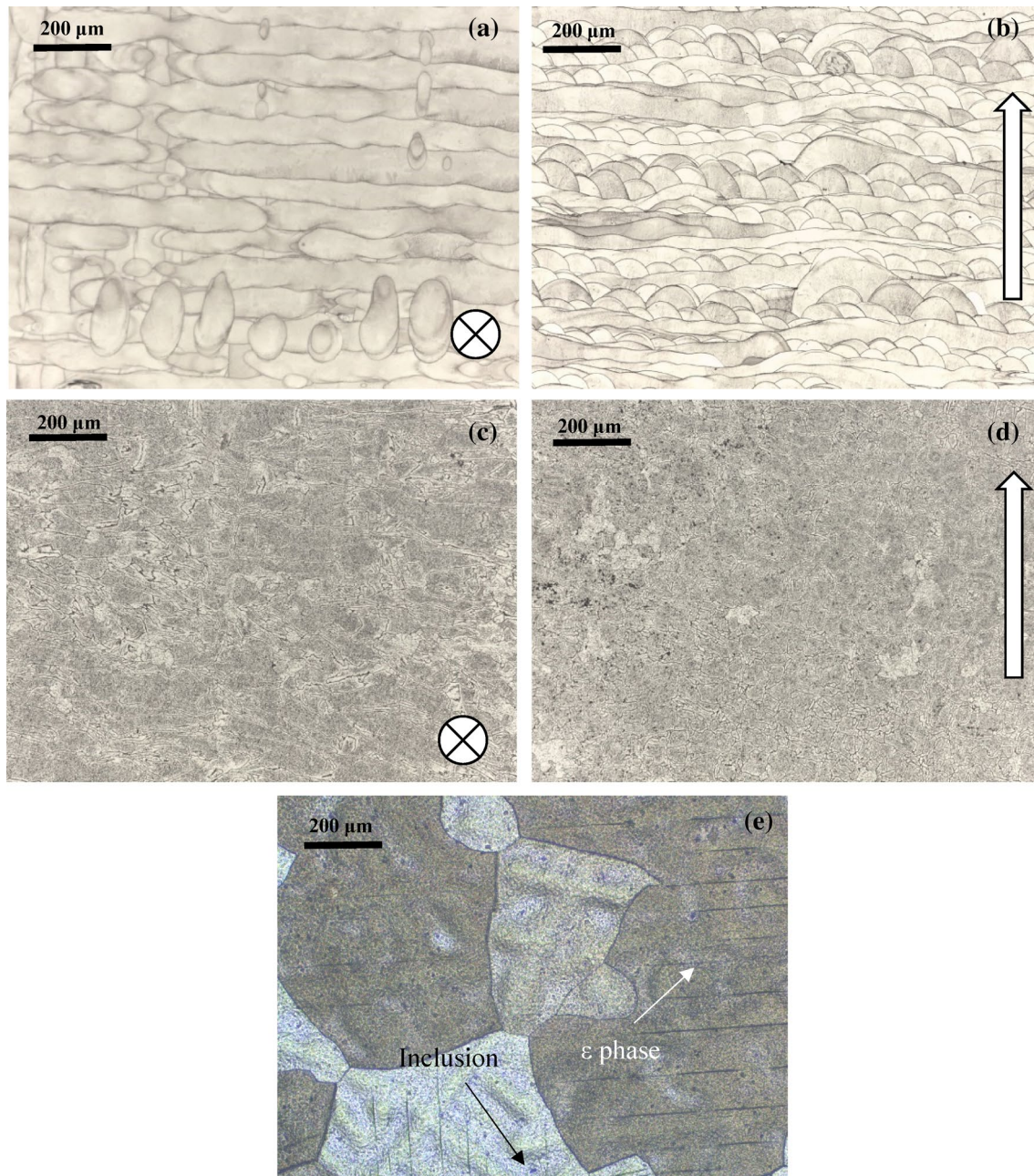
Fig. 5 Optical microscopy images of **a** as-printed sample in the horizontal direction, **b** as-printed sample in the vertical direction, **c** heat-treated sample in the horizontal dir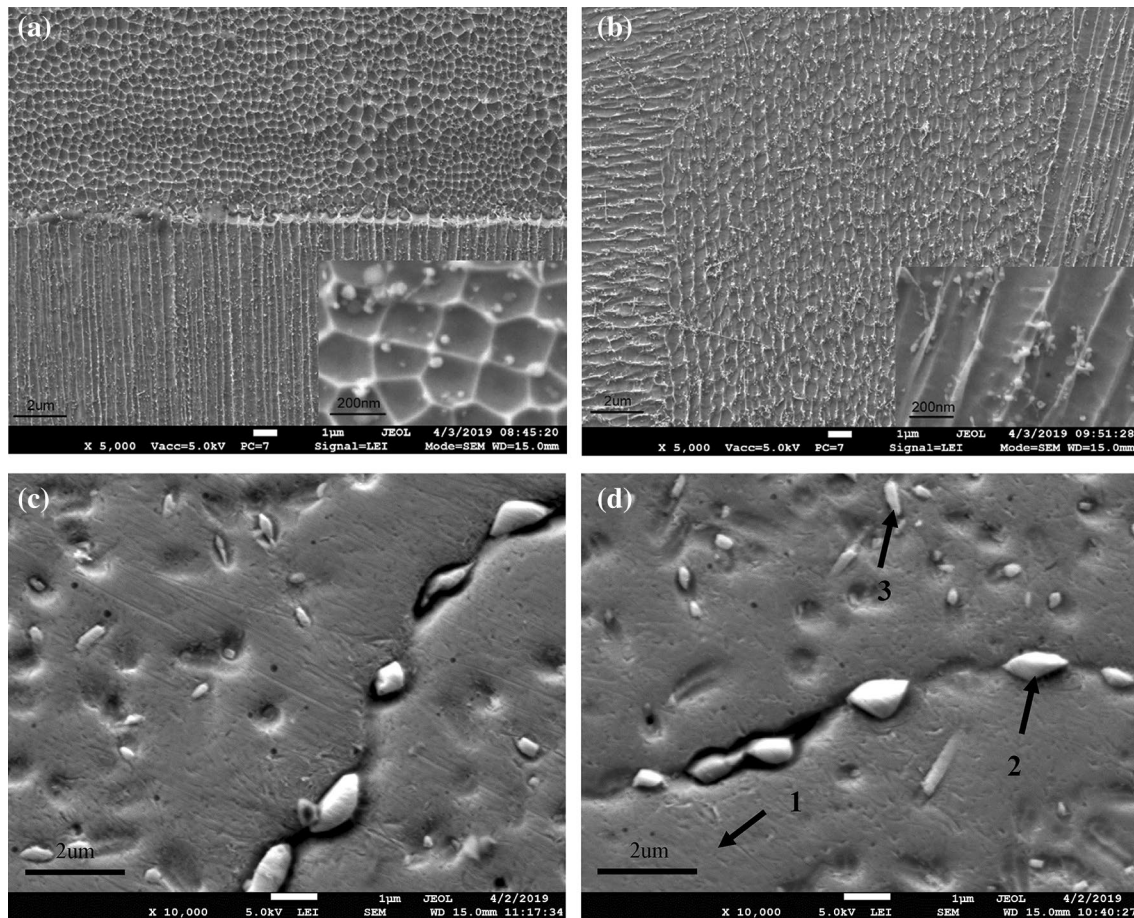ection, **d** heat-treated sample in the vertical direction, and **e** wrought sample (reference). The symbols indicate the growth direction

of the grains. The precipitates mainly consisted of W and Si (Table 5). Those precipitates observed at the boundaries were richer in W (site 2) than those observed in the interior of the cells (site 3).

The horizontal samples in both the as-printed and heat-treated conditions were characterized by SKPFM in order to determine the difference in the Volta potentials of the metal matrix, precipitates visible in Fig. 6, and surrounding matrix

(Fig. 7). The Volta potential maps of the reference wrought material were also acquired.

The Volta potential maps, acquired by SKPFM technique, highlight the presence of small cathodic regions in the 3D printed samples, while the Volta potential is almost flat in the wrought material. It is likely that the cathodic regions, observed in the 3D printed materials, correspond to the Si-W precipitates observed in FE-SEM images (Fig. 6). The cathodic regions appear more evident in the heat-treated

Fig. 6 FE-SEM images of the additively manufactured samples. **a** As-printed in the horizontal direction (with a zoom-in image at higher magnifications), **b** as-printed in the vertical direction (with a zoom-in image at higher magnifications), **c** heat-treated in the horizontal direction and d) heat-treated in the vertical direction

Table 5 Semi-quantitative chemical analysis results for the sites indicated in Fig. 6 (wt.%), as obtained using EDXS (point analysis)

	Si	Cr	W	Co
Site 1 (matrix)	1 ± 0.2	26.4 ± 0.5	7.3 ± 0.1	Bal
Site 2 (Grain boundary precipitate)	1.9 ± 0.15	9.4 ± 0.3	51.0 ± 0.5	Bal
Site 3 (internal precipitate)	2.2 ± 0.11	16.4 ± 0.3	39.2 ± 0.4	Bal

sample than in the as-printed sample. Therefore, it is likely that the heat treatment slightly increases the Volta potential difference between the Si-W precipitates and the metal matrix. In the as-printed material, the Volta potential difference between the precipitates and the matrix is only few mV, it is 30–50 mV after heat treatment. This increase of the Volta potential difference is probably due to the increase of elemental partition in the precipitates during thermal treatment. However, the Volta potential difference was very small for all the samples. It can be expected that these small

potential differences did not significantly affect the corrosion behavior of the L-PBF samples after the post-heat treatment.

As can be observed from Table 6, the hardness of the as-printed material was slightly higher than those of the heat-treated additively manufactured samples. This is because the heat-treated samples had coarser precipitates, in lower amount. The building direction seems to not have effect on the hardness of the samples. In contrast, the hardness of the additively manufactured materials was considerably higher than that of the wrought materials because of both the presence of precipitates and the finer microstructure resulting from the L-PBF process.

3.2 Corrosion testing

CoCrW alloys are widely used for developing human implants, which should be resistant to attack from aggressive body fluids even in the presence of crevices. For this reason, corrosion tests were performed under both the neutral and acidic conditions. The acidic conditions
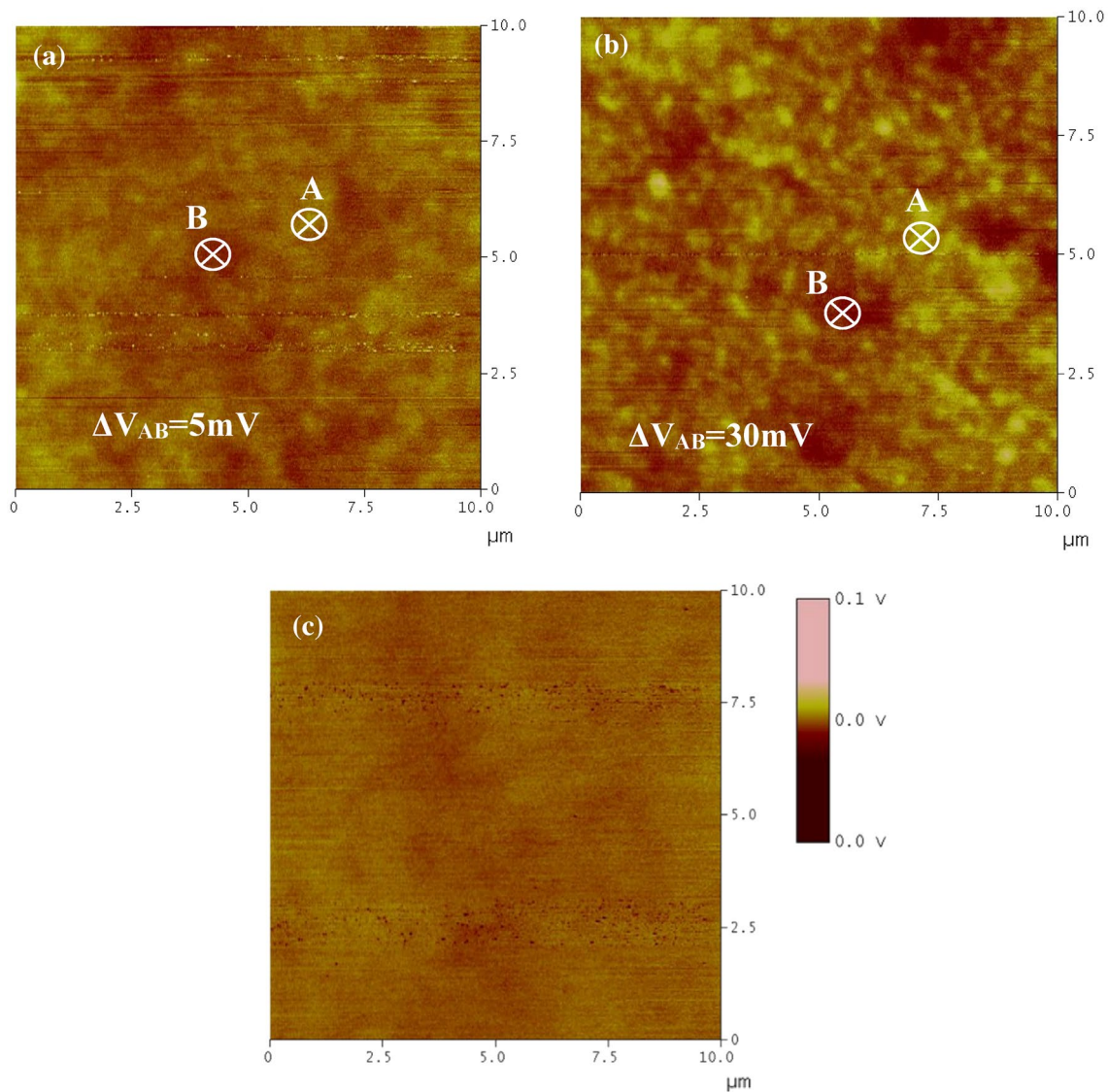
Fig. 7 SKPFM Volta potential maps for the **a** additively manufactured horizontal sample in the as-printed condition, **b** additively manufactured horizontal sample in the heat-treated condition, **c** wrought sample. The pointers A (precipitate) and B (matrix) indicate the most cathodic and anodic sites in the map, respectively

**Table 6** Hardness (HV2) of the L-PBF and wrought samples

Type of sample	Horizontal	Vertical
As-printed L-PBF	420 ± 12	418 ± 16
Heat-treated L-PBF	408 ± 10	406 ± 8
Wrought	280 ± 5 (no preferential direction)	

were used to investigate the behavior of the CoCrMo alloy in an acidic environment, which is typically observed in crevices formed during the installation of modular human prosthesis, such as a modular hip prosthesis. As is well known [4], crevices can locally acidify human body fluids.

Moreover, local acidification can also be caused by inflammatory processes [1, 3, 4].

The potentiodynamic curves obtained from the tested materials immersed in the 9 g/L NaCl solution at pH = 7 and 2 are shown in Fig. 8.

The potentiodynamic curves obtained in the neutral solution (Fig. 8a) showed that both the heat-treated and as-printed L-PBF samples exhibited a similar passive behavior with a passive current of $5.1 \times 10^6 \pm 0.2$ (A/cm^2). The anodic current density increased significantly at approximately 0.8 ± 0.1 V vs. Ag/AgCl because of the electrochemical dissolution of the passive film (transpassive potential). No significant difference was observed in the curves obtained for the materials built in
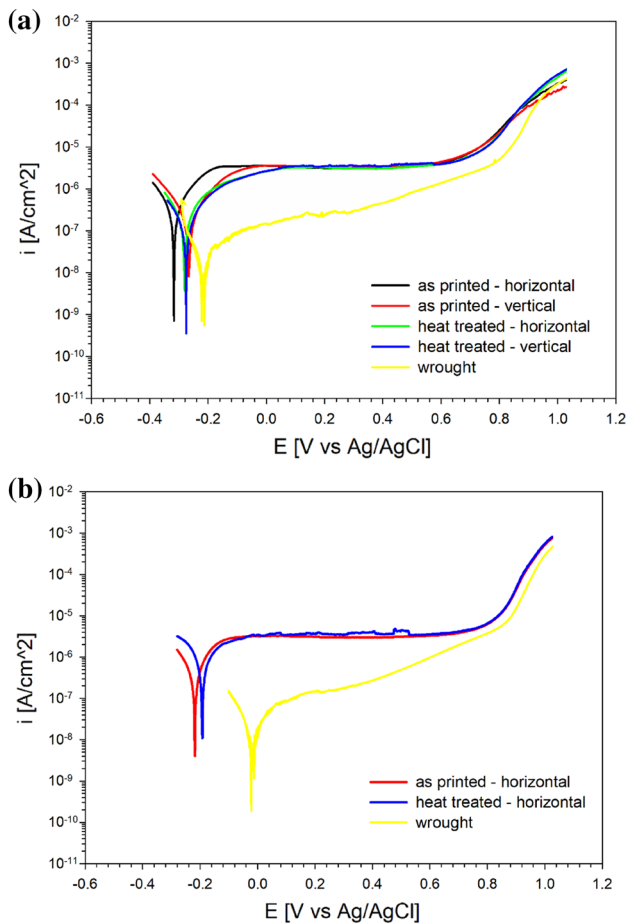
Fig. 8 Potentiodynamic curves of the specimens in the aqueous 9 g/L NaCl solution at **a** pH = 7 and **b** pH = 2

the vertical and horizontal directions, indicating that the building direction did not significantly affect the corrosion behavior of the L-PBF samples. The curve for the wrought material exhibited a passive behavior similar to that of the L-PBF materials. The corrosion potential of the wrought alloy was similar to those of the additively manufactured materials. However, its corrosion current density and the current density in the passive range were lower than those of the additively manufactured materials. This can be attributed to the absence of discontinuities, such as pores, unmelted particles, and precipitates, in the wrought material [35]. Because the printing direction did not affect the electrochemical behavior of the samples in the neutral solution (Fig. 8a), the potentiodynamic curves in the acidic solution were recorded only for the horizontal direction of the L-PBF samples and for the reference wrought alloy (Fig. 8b). The overall behavior of the L-PBF and wrought samples was confirmed by their polarization curves obtained in the electrolyte with pH = 2. In particular, it was confirmed that the as-printed and heat-treated L-PBF CoCrW samples showed similar behaviors. The

behavior of the wrought material at pH = 2 was similar to that observed at pH = 7. It was found that, in both the corrosive media, the alloys retained their passivity, also in conditions that simulated the presence of crevices in human implants (pH = 2) [4].

The SEM images of the surfaces of the L-PBF and wrought samples after the potentiodynamic polarization in the neutral solution are shown in Fig. 9. The L-PBF CoCrW alloy showed a localized dissolution near the pores or unmelted/partially melted particles in both the as-printed and heat-treated conditions, although these defects are present in low amounts (see arrows in Fig. 9) [36]. It is likely that in these areas the passive film can be weaker because of surface alteration and the presence of microstructural discontinuities. Considering the low amount of pores, these small defects are usually present in the 3D printed material and are not linked to the optimized printing conditions that are well optimized [13]. The Si-W-rich particles, the unique precipitates found in this material, as well as grain boundaries were well highlighted by electrochemical dissolution of passive film in the heat-treated alloys (more evident for the samples polarized in the acidic solution), resulting in metallographic etching, which was not observed in the as-printed L-PBF samples, caused by the electrochemical stripping of passive layer on metal matrix (above transpassivity potential). It is to evidence that the material dissolution occurred in a more intense way around unmelted particles or pores (Fig. 9 indicated by arrows) respect to the dissolution around precipitates. Apart from this slightly difference in corrosion morphologies, no significant difference was observed between the electrochemical behaviors of the as-printed and heat-treated samples.

Unlike the L-PBF samples, the wrought CoCrW alloy exhibited only very small pits, which probably nucleated close to very small inclusions typically present in the material [37, 38].

The morphology of the samples polarized in the acid electrolyte was similar to that of the samples polarized in the neutral solution (Fig. 9).

The potentiodynamic polarization curves in Fig. 8 and the morphologies shown in Fig. 9 indicate that the L-PBF and wrought CoCrW alloys showed a stable passive film in both the test environments. The samples prepared in this study showed a wide passive range, indicating that the samples exhibited high corrosion resistance.

3.3 Dry and wet-wear tests

Wear tests were performed under dry conditions at room temperature to investigate the relationship between the tribological behavior and microstructures of the L-PBF and wrought samples. Moreover, wear tests were carried out under wet conditions, because CoCrW alloys are often
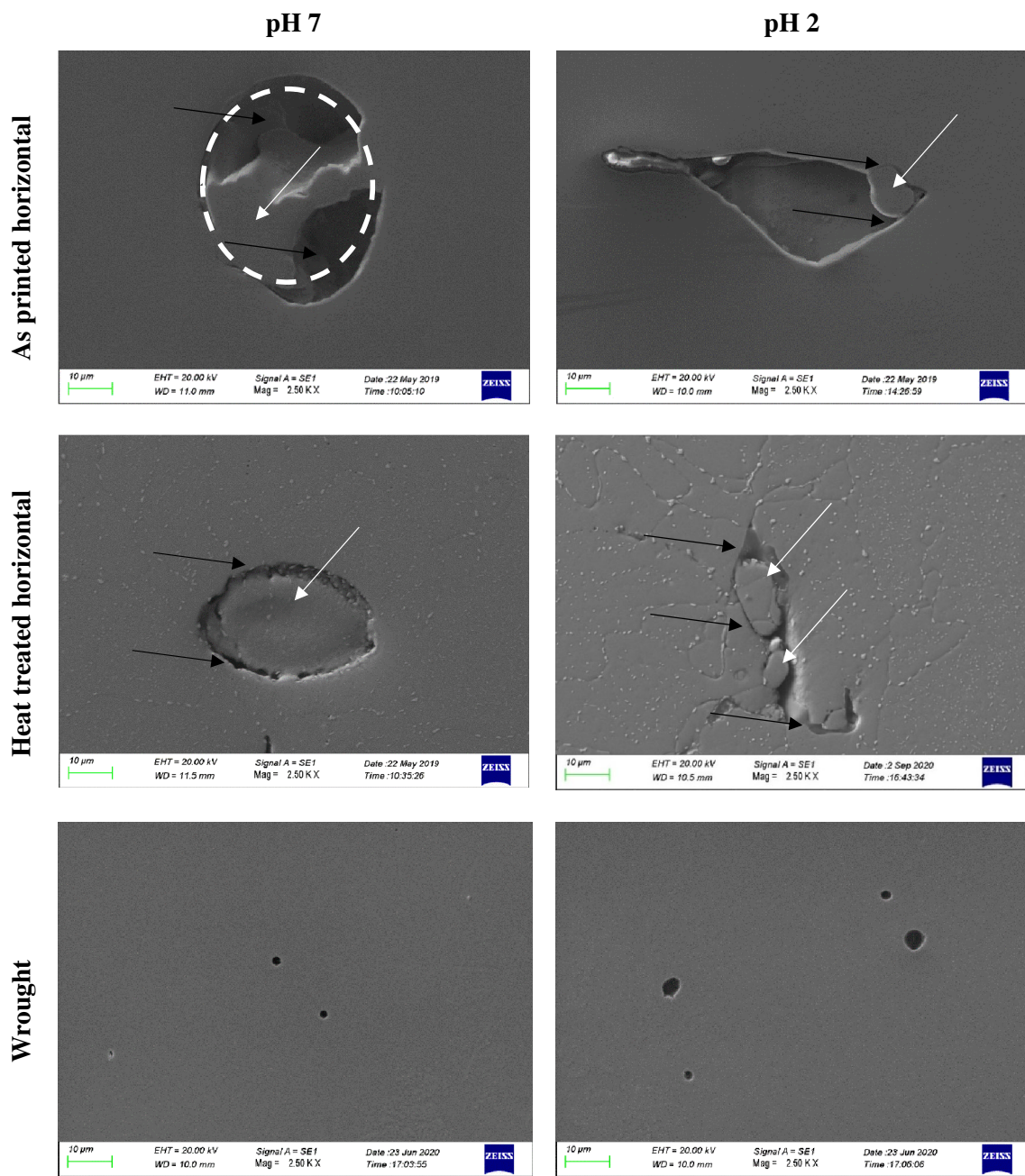
Fig. 9 Corrosion morphologies of the specimens after the potentiodynamic tests in the aqueous media with 9 g/L NaCl at pH = 7 and 2. For the additively manufactured materials only, the results obtained for the horizontal samples are shown. White arrows indicate the unmelted particles, black arrows indicate the dissolved material

applied in human implants and exhibit wear degradation under mechanical and chemical effects [1, 3]. The wet and dry tests of the samples were carried out using the same experimental procedure. In the wet-wear test, the CoCrW samples were immersed for 15 min in the media same as those used for the electrochemical tests using the tribometer cell prior to the mechanical test.

Figure 10 shows the wear performances of the specimens tested at the stroke length of 10 mm and the worn areas for the specimens tested at the stroke length of 0.2 mm under the dry and wet conditions (neutral and acidic electrolytes).

The additively manufactured alloys exhibited higher wear resistance than the wrought material when the stroke length of 10 mm was used. This behavior of the additively manufactured materials can be attributed to their microstructure, which consisted of a fine gamma phase and small Si-W intermetallics. On the other hand, the wrought material exhibited coarse grains as compared to the L-PBF

Fig. 10 Wear rates of the materials tested in different tribological environments at the stroke length of **a** 10 mm **b** 0.2 mm. *NT* not treated, *T* post-heat treatment, reference = wrought. The presented data are an average value, the error bars represent the standard deviation of these measurements
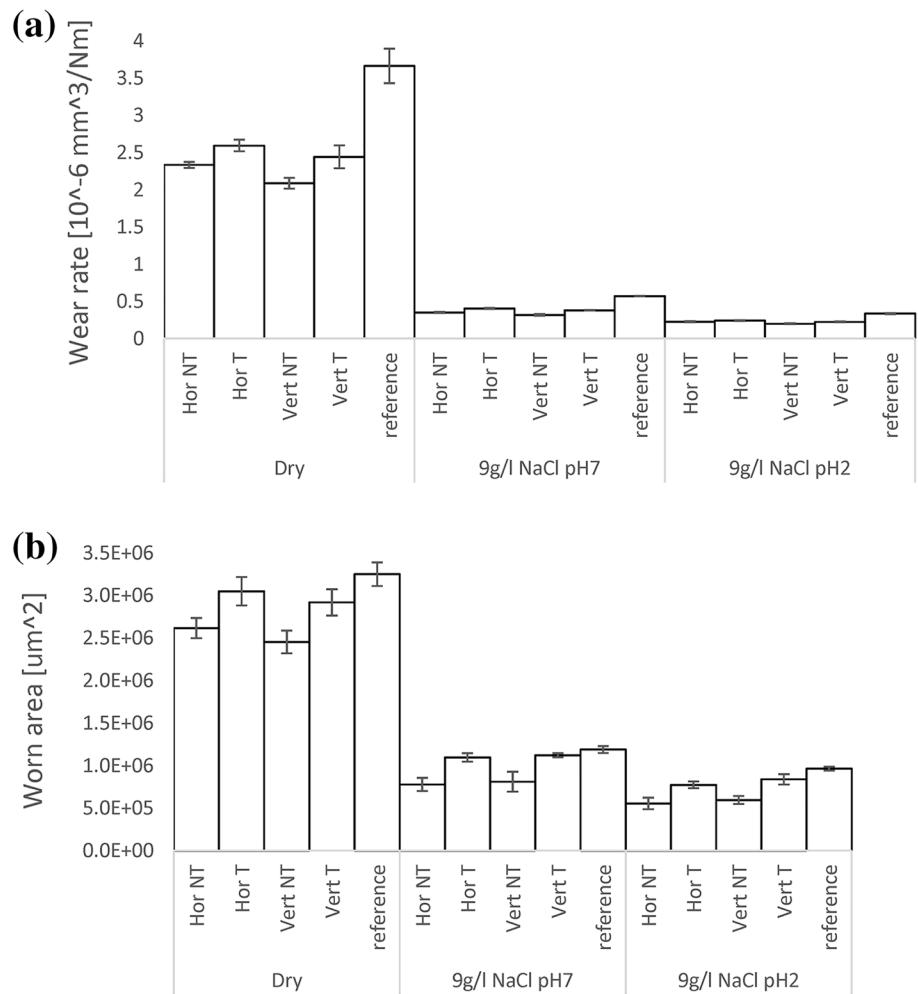

alloys owing to their lower hardness. In addition, the wear tests highlighted the anisotropy of the additively manufactured samples. In particular, the horizontal samples showed slightly low wear resistance as compared to the vertical samples. This behavior has also been observed by other researchers for different materials, mainly when Hertzian stresses are very low [39]. Another important observation is that the heat treatment slightly decreased the wear resistance of the L-PBF material. This is related to the microstructural evolution of the material during the heat treatment, which led to the coarsening of the intermetallic W-Si precipitates and the consequent decrease in the material hardness. However, the wear resistance of the heat-treated additively manufactured material was still higher than that of the wrought material. The results obtained under the wet conditions exhibited trends similar to those obtained under the dry conditions. However, the wear rate of the samples decreased significantly under the wet conditions. Mechanical wear was likely the main degradation mechanism of the samples under the wet

conditions. The contribution of the corrosion processes on the CoCrW alloys was very limited owing to their strong passive behavior. This behavior is in line with the wet wear tests results reported previously for materials prepared using conventional methods [32, 40, 41].

To further investigate the wear mechanism of the as-printed horizontal samples, the top-view SEM images of their worn areas were obtained (Fig. 11).

A detailed analysis of the wear tracks showed that abrasion was very intense under dry conditions (in both sliding conditions) and attenuated in the wet-wear tests, mainly at pH = 2. This can mainly be attributed to the washing effect of the aqueous media, which tended to remove the debris produced during the wear contact on the wear track. At pH = 2, the further reduction of the abrasive wear mechanism can be attributed to the probable partial dissolution of the small wear debris produced during the tribocontact. The morphology of the wear tracks further confirmed that the main wear mechanism in the samples was abrasion. As mentioned earlier, the effect of corrosion in the wet wear

Stroke length of 10 mm   **Stroke length of 0.2 mm**
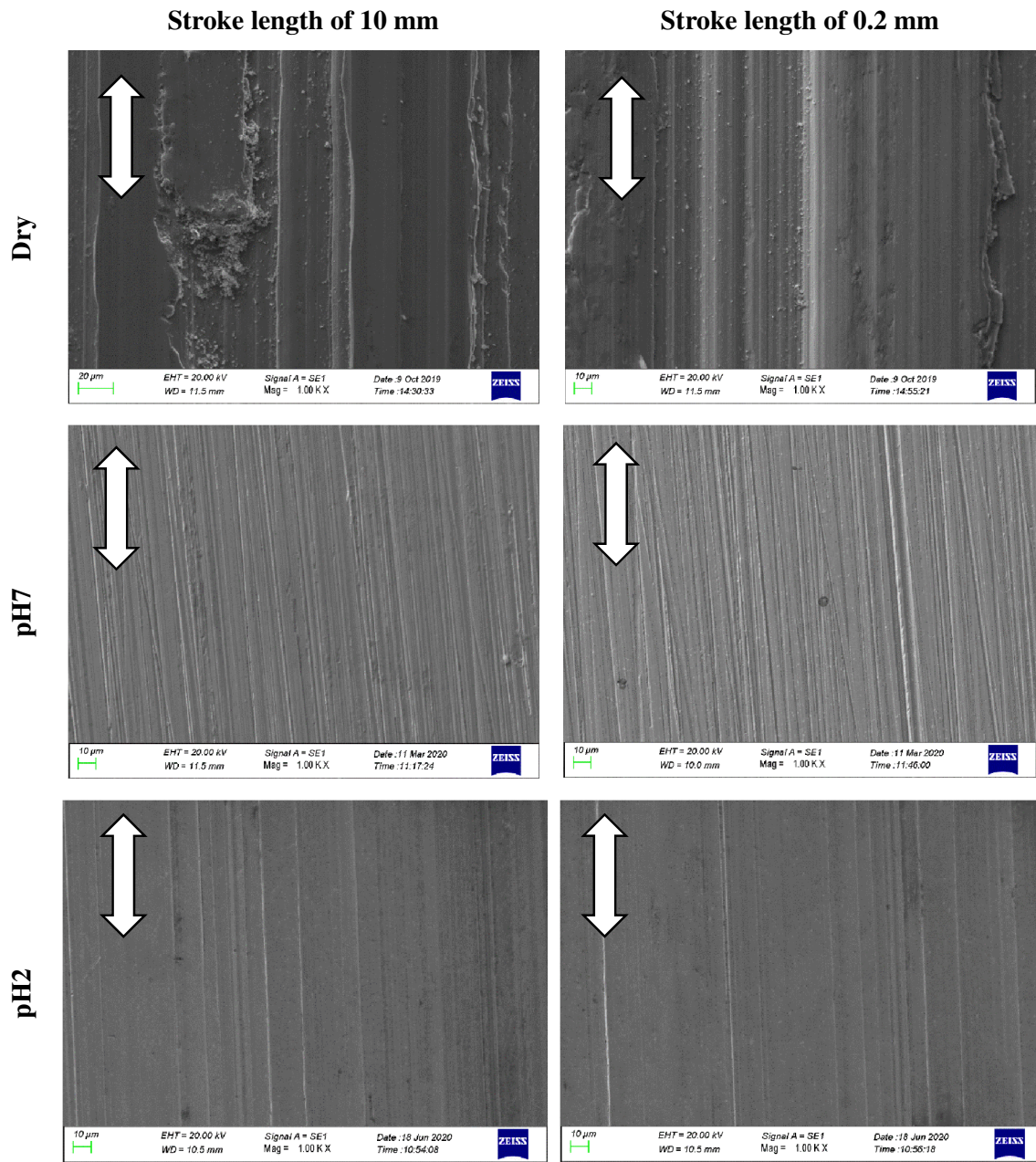
Fig. 11 SEM images of the worn areas of as-printed horizontal specimens at different stroke lengths and under different test environments. The arrows indicate the sliding direction

tests was negligible, and no morphological degradation attributing to the corrosion process was observed (formation of pits, selective corrosion, etc.).

4 Conclusions

In this study, we investigated the effect of thermal treatment on the corrosion behavior and wet wear performance of additively manufactured CoCrW alloys.

The as-printed CrCoW alloy showed a fine-grained cellular/microcolumnar microstructure with very small Si-W precipitates, which contributed to its improved hardness as compared to that of the forged alloy, and are produced by a segregative process at cell/columns boundaries. Solubilization at 1150 °C led to a clear modification of the microstructure with grain size growth and coarsening of the Si-W precipitates. The heat-treated additively manufactured samples, from a qualitative evaluation, showed slightly lower hardness than the as-printed samples.

The L-PBF material exhibited a passive behavior similar to that of the wrought alloy. The anodic currents of the L-PBF samples were higher than those of the wrought alloy, indicating the higher heterogeneity of the microstructure of the L-PBF samples. This can be attributed to the presence of some small defects (voids and pores) originating from the technological process in the L-PBF samples. The thermal treatment did not significantly affect the corrosion behavior of the samples, although precipitates were observed when the passive layer was removed. The material corroded mainly in the proximity of the unmelted particles or pores.

In both the dry and wet conditions, the wear resistance of the additively manufactured samples was strongly related to their hardness (mechanical properties). The heat-treated samples exhibited low wear resistance as compared to the as-printed samples. However, the wear resistance of the CoCrW alloy produced by L-PBF was higher than that of its wrought counterpart. The main wear mechanism of the samples was abrasive wear, which attenuated in the wet wear tests, particularly in the acidic medium.

Data availability The raw/processed data required to reproduce these findings cannot be shared at this time as the data also forms part of an ongoing study.

References

1. Manam NS, Harun WSW, Shri DNA et al (2017) Study of corrosion in biocompatible metals for implants: a review. J Alloys Compd 701:698–715. https://doi.org/10.1016/j.jallcom.2017.01.196

2. Arnholt CM, Macdonald DW, Malkani AL et al (2016) Corrosion damage and wear mechanisms in long-term retrieved CoCr femoral components for total knee arthroplasty. J Arthroplasty 31:2900–2906. https://doi.org/10.1016/j.arth.2016.05.006

3. Asri RIM, Harun WSW, Samykano M et al (2017) Corrosion and surface modification on biocompatible metals: a review. Mater Sci Eng C 77:1261–1274. https://doi.org/10.1016/j.msec.2017.04.102

4. Lanzutti A, Andreatta F, Rossi L et al (2019) Corrosion fatigue failure of a high carbon CoCrMo modular hip prosthesis: failure analysis and electrochemical study. Eng Fail Anal 105:856–868. https://doi.org/10.1016/j.engfailanal.2019.07.044

5. Sarantopoulos DM, Beck KA, Holsen R, Berzins DW (2008) Corrosion of CoCr and NiCr dental alloys alloyed with palladium. J Prosthet Dent 105:35–43. https://doi.org/10.1016/S0022-3913(10)60188-6

6. Hedberg YS, Qian B, Shen Z et al (2014) In vitro biocompatibility of CoCrMo dental alloys fabricated by selective laser melting. Dent Mater 30:525–534. https://doi.org/10.1016/j.dental.2014.02.008

7. Won H, Jung K, Hwang S et al (2019) Microstructure and mechanical anisotropy of CoCrW alloy processed by selective laser melting. Mater Sci Eng A 749:65–73. https://doi.org/10.1016/j.msea.2019.02.013

8. Gong X, Li Y, Nie Y et al (2018) Corrosion behaviour of CoCrMo alloy fabricated by electron beam melting. Corros Sci 139:68–75. https://doi.org/10.1016/j.corsci.2018.04.033

9. Wang Y, Yan Y, Su Y, Qiao L (2017) Release of metal ions from nano CoCrMo wear debris generated from tribo-corrosion processes in artificial hip implants. J Mech Behav Biomed Mater 68:124–133. https://doi.org/10.1016/j.jmbbm.2017.01.041

10. Lu Y, Guo S, Yang Y et al (2018) Effect of thermal treatment and fluoride ions on the electrochemical corrosion behavior of selective laser melted CoCrW alloy. J Alloys Compd 730:552–562. https://doi.org/10.1016/j.jallcom.2017.09.318

11. Song C, Zhang M, Yang Y et al (2018) Morphology and properties of CoCrMo parts fabricated by selective laser melting. Mater Sci Eng A 713:206–213. https://doi.org/10.1016/j.msea.2017.12.035

12. Lu Y, Wu S, Gan Y et al (2015) Investigation on the microstructure, mechanical property and corrosion behavior of the selective laser melted CoCrW alloy for dental application. Mater Sci Eng C 49:517–525. https://doi.org/10.1016/j.msec.2015.01.023

13. Lu Y, Ren L, Wu S et al (2018) CoCrWCu alloy with antibacterial activity fabricated by selective laser melting: Densification, mechanical properties and microstructural analysis. Powder Technol 325:289–300. https://doi.org/10.1016/j.powtec.2017.11.018

14. Lu Y, Xu X, Yang C et al (2020) In vitro insights into the role of copper ions released from selective laser melted CoCrW-x Cu alloys in the potential attenuation of inflammation and osteoclastogenesis. J Mater Sci Technol 41:56–67. https://doi.org/10.1016/j.jmst.2019.09.016

15. Kajima Y, Takaichi A, Nakamoto T, Kimura T (2016) Fatigue strength of Co–Cr–Mo alloy clasps prepared by selective laser melting. J Mech Behav Biomed Mater 59:446–458. https://doi.org/10.1016/j.jmbbm.2016.02.032

16. Hitzler L, Alifui-segbaya F, Williams P et al (2018) Additive manufacturing of cobalt-based dental alloys: analysis of microstructure and physicomechanical properties. Adv Mater Sci and Eng 2018:1–12

17. Wang D, Ye G, Dou W et al (2020) Influence of spatter particles contamination on densification behavior and tensile properties of CoCrW manufactured by selective laser melting. Opt Laser Technol 121:105678. https://doi.org/10.1016/j.optlastec.2019.105678

18. Dimitriadis K, Lekatou AG, Sfikas AK et al (2021) Influence of heat-treatment cycles on the microstructure, mechanical

properties, and corrosion resistance of Co–Cr dental alloys fabricated by selective laser melting. J Mater Eng Perform 30:5252–5265. https://doi.org/10.1007/s11665-021-05738-9

19. Sing SL, Huang S, Yeong WY (2020) Effect of solution heat treatment on microstructure and mechanical properties of laser powder bed fusion produced cobalt-28chromium-6molybdenum. Mater Sci Eng A 769:138511. https://doi.org/10.1016/j.msea.2019.138511

20. Cui G, Liu H, Li S et al (2019) Design and high-temperature tribological properties of CoCrW with rare earth fluoride. Integr Med Res 9:2402–2411. https://doi.org/10.1016/j.jmrt.2019.12.072

21. Guadalupe S, Cao S, Cantoni M et al (2017) Applicability of a recently proposed tribocorrosion model to CoCr alloys with different carbides content. Wear 376–377:203–211. https://doi.org/10.1016/j.wear.2016.11.048

22. Luo J, Wu S, Lu Y et al (2018) The effect of 3 wt% Cu addition on the microstructure, tribological property and corrosion resistance of CoCrW alloys fabricated by selective laser melting. J Mater Sci Mater Med. https://doi.org/10.1007/s10856-018-6043-7

23. Qiu J, Yu WQ, Ohang FQ et al (2011) Corrosion behaviour and surface analysis of a Co–Cr and two Ni–Cr dental alloys before and after simulated porcelain firing. Eur J Oral Sci 119:93–101. https://doi.org/10.1111/j.1600-0722.2011.00791.x

24. Xin XZ, Chen J, Xiang N et al (2014) Surface characteristics and corrosion properties of selective laser melted Co–Cr dental alloy after porcelain firing. Dent Mater 30:263–270. https://doi.org/10.1016/j.dental.2013.11.013

25. De Graeve I, Schoukens I, Lanzutti A et al (2013) Mechanism of corrosion protection of hot-dip aluminium-silicon coatings on steel studied by electrochemical depth profiling. Corros Sci. https://doi.org/10.1016/j.corsci.2013.07.005

26. Lanzutti A, Andreatta F, Magnan M, Fedrizzi L (2018) Microstructural and in-depth electrochemical characterization of Zn diffusion layers on aluminum 3xxx alloy. Surf Interface Anal. https://doi.org/10.1002/sia.6602

27. Merdji A, Bachir Bouiadjra B, Ould Chikh B et al (2012) Stress distribution in dental prosthesis under an occlusal combined dynamic loading. Mater Des 36:705–713. https://doi.org/10.1016/j.matdes.2011.12.006

28. Lanzutti A, Lekka M, De LC, Fedrizzi L (2019) Tribology international effect of pulse current on wear behavior of Ni matrix micro-and nano-SiC composite coatings at room and elevated temperature. Tribol Int 132:50–61. https://doi.org/10.1016/j.triboint.2018.12.011

29. Lanzutti A (2013) Tribological behavior of thermal spray coatings, deposited by HVOF and APS techniques, and composite electrodeposits Ni/SiC at both room temperature and 300 °C. Tribol Ind. 35:113–122

30. Regis M, Lanzutti A, Bracco P, Fedrizzi L (2018) Wear behavior of medical grade PEEK and CFR PEEK under dry and bovine serum conditions. Wear. https://doi.org/10.1016/j.wear.2018.05.005

31. Lanzutti A, Raffaelli A, Magnan M et al (2019) Microstructural and mechanical study of an induction nitrided Ti gr .5 hip prosthesis component. Surf Coat Technol 377:124895. https://doi.org/10.1016/j.surfcoat.2019.124895

32. Vieira AC, Ribeiro AR, Rocha LA, Celis JP (2006) Influence of pH and corrosion inhibitors on the tribocorrosion of titanium in artificial saliva. Wear 261:994–1001. https://doi.org/10.1016/j.wear.2006.03.031

33. Cao L (2020) Mesoscopic-scale simulation of pore evolution during laser powder bed fusion process. Comput Mater Sci 179:109686. https://doi.org/10.1016/j.commatsci.2020.109686

34. Yamanaka K, Mori M, Chiba A (2014) Dynamic recrystallization of a biomedical Co–Cr–W-based alloy under hot deformation. Mater Sci Eng A 592:173–181. https://doi.org/10.1016/j.msea.2013.11.002

35. Man C, Dong C, Liu T et al (2019) The enhancement of microstructure on the passive and pitting behaviors of selective laser melting 316L SS in simulated body fluid. Appl Surf Sci 467–468:193–205. https://doi.org/10.1016/j.apsusc.2018.10.150

36. Suryawanshi J, Baskaran T, Prakash O et al (2018) On the corrosion resistance of some selective laser melted alloys. Materialia 3:153–161. https://doi.org/10.1016/j.mtla.2018.08.022

37. Reclaru L, Lu H, Eschler P et al (2005) Corrosion behaviour of cobalt—chromium dental alloys doped with precious metals. Biomaterials 26:4358–4365. https://doi.org/10.1016/j.biomaterials.2004.11.018

38. Souza KS, Flavia R, Villamil V, Rogero SO (2016) In vitro cytotoxicity test and surface characterization of CoCrW alloy in artificial saliva solution for dental applications. Braz Dent J 27:181–186

39. Yang Y, Zhu Y, Khonsari MM, Yang H (2019) Wear anisotropy of selective laser melted 316L stainless steel. Wear 428–429:376–386. https://doi.org/10.1016/j.wear.2019.04.001

40. Mathew MT, Abbey S, Hallab NJ et al (2012) Influence of pH on the tribocorrosion behavior of CpTi in the oral environment: synergistic interactions of wear and corrosion. J Biomed Mater Res. https://doi.org/10.1002/jbm.b.32735

41. Royhman D, Patel M, Runa MJ et al (2016) Fretting-corrosion behavior in hip implant modular junctions: the influence of friction energy and pH variation. J Mech Behav Biomed Mater 62:570–587. https://doi.org/10.1016/j.jmbbm.2016.05.024